SCIENCE CHINA
Technological Sciences

•Article•

March 2024 Vol.67 No.3: 853–862
https://doi.org/10.1007/s11431-023-2437-7

Increasing operational stability of journal bearing in hydraulic suspension micro-pump by herringbone grooved structure

HONG Tao, XING GuanYing, ZUO HuaiYu, XUE Song & LUO XiaoBing*

State Key Laboratory of Coal Combustion, School of Energy and Power Engineering, Huazhong University of Science and Technology, Wuhan 430074, China

Received January 9, 2023; accepted May 22, 2023; published online February 6, 2024

The operational stability of radial journal bearings is the bottleneck that limits the reliability of hydraulic suspension micro-pump. Due to self-excited vibrations, the whirl amplitude of the plain journal bearing (PJB) is large at high rotational speeds, which will accelerate wear failure. It has been proven that employing herringbone grooved journal bearing (HGJB) is an effective method to reduce the whirl amplitude and improve operational stability. However, enhancing the stability of journal bearings in micro-pumps by herringbone grooved structures has rarely been studied, and its effect needs to be verified. We validated the mechanism of the stability improvement with the CFD method and compared the dynamic characteristics of HGJB and PJB by rotor dynamics evaluation and experiment. The experimental results show that under the same conditions the whirl amplitude of the HGJB decreases by 29.61% in the x direction and by 24.09% in the y direction compared with that of the PJB. This study reveals the effect of the herringbone grooved structure on the operational stability of bearings and may provide guidance for the reliability improvement of hydraulic suspension micro-pump.

journal bearing, herringbone groove, hydrodynamic effect, micro-pump

Citation: Hong T, Xing G Y, Zuo H Y, et al. Increasing operational stability of journal bearing in hydraulic suspension micro-pump by herringbone grooved structure. Sci China Tech Sci, 2024, 67: 853–862, https://doi.org/10.1007/s11431-023-2437-7

1 Introduction

A micro-pump is the power source of microfluidic delivery, which is widely used in the fields of drug delivery [1,2], artificial hearts [3,4], electronic cooling systems [5–8], etc., and has broad application prospects [9]. According to the difference in working principles, micro-pumps can be divided into piezoelectric pumps [10], electroosmotic pumps [11], electrohydrodynamic pumps [12], and centrifugal pumps [13,14]. Among them, centrifugal pumps have the advantages of high hydraulic performance and good adjustability; thus, they have become a promising choice for driving microfluidic systems. Centrifugal pumps can be divided into contact bearing pumps and suspension bearing pumps according to the supporting mode of the rotor [15,16]. The problem of the contact bearing pump is mechanical friction, which restricts the reliability and endurance in application [16,17]. To prevent contact wear problems, we developed a kind of hydraulic suspension micro-pump with a radial journal bearing in our previous studies [18,19]. The hydrodynamic effect makes the rotating components levitate, which prevents contact with other components, thus greatly improving the theoretical life of the micro-pump.

The radial suspension bearing used in this micro-pump is essentially a plain journal bearing (PJB), which is widely used in rotating machines. The journal is set eccentrically relative to the bearing, and the liquid film in the convergence zone produces a dynamic pressure effect when the journal rotates. This pressure balances the load on the journal and separates the journal from the inner wall of the bearing.

*Corresponding author (email: luoxb@hust.edu.cn)

However, the supporting force produced by the liquid film is not collinear with the eccentric direction of the journal, causing a moment that will promote the whirl of the journal. The moment will generate self-excited vibrations at high speeds, and the journal will no longer be in a steady state. As a result, when the whirl amplitude increases, collisions between the journal and bearing may occur, seriously affecting the performance and reliability of the pump. At present, researchers have carried out a series of studies on increasing PJB operational stability. Kumar et al. [20] and Garg et al. [21] found that the viscosity of the lubricant has a significant influence on the dynamic characteristics of a PJB, and the use of magnetic fluids or certain non-Newtonian fluids can improve the operational stability of a PJB. However, the fluid choice depends on the function of the microfluidic system, making the viscosity change impractical. Alternatively, adding external support, such as that used in floating ring bearings, provides an effective means for increasing operational stability. The bearing is installed on the external film with appropriate damping, which can absorb vibration energy and greatly reduce the whirl amplitude of the bearing [22]. However, external support will inevitably reduce the power density and increase the complexity of the system. In addition, reducing the bearing width has also been proven to be an effective method to improve operational stability [23]. Nonetheless, simply reducing the width will increase the end leakage and decay the loading performance of the journal bearing. In addition, the motor design determines the width of the rotor, thus limiting the structure optimization of the journal suspension. In summary, the three methods mentioned above are not applicable to hydraulic suspension micro-pump. In recent years, the method of machining microgrooves on the journal surface has become an effective means to improve the stability of journal bearings due to its advantages of reliability and efficiency, which can improve operational stability by strengthening the local hydrodynamic effect [24]. To date, grooved bearings have been widely used in bearings with gas, liquid, and grease as lubricants, especially in miniaturized bearings [25–27].

Among the various shapes of grooves, the herringbone groove, which can suppress whirl instability, has aroused widespread attention. The mechanism can be explained as follows: when the journal rotates, the groove restricts the flow of fluids, which causes the fluids to converge at the cusp, forming a pumping effect [24], thus enhancing the local pressure and improving the dynamic characteristics of the journal bearing. Narrow groove theory (NGT) has been proposed to investigate the suspension characteristics of a herringbone grooved journal bearing (HGJB) [28,29], which assumes that the number of grooves is infinite, while for an HGJB with finite slots, its accuracy is unsatisfying. Alternatively, the finite difference method (FDM) [23,30,31] and finite element method (FEM) [32,33] are used to solve the nonlinear Reynolds equation numerically and are sufficiently accurate compared with the experiments. Furthermore, Hirs [34] and Gao et al. [35] experimentally studied a hydrodynamic HGJB and an aerostatic HGJB and obtained better stability than a PJB. In addition, an HGJB can significantly restrain the radial runout of the high-speed spindle and increase the maximum operating speed [36]. Due to its excellent dynamic properties, HGJBs have been used in high-speed light-load rotating machinery, such as high-precision machine tool spindles and hard disks. Moreover, there are few studies that use herringbone grooves to improve the stability of radial suspension bearings in micro-pump. Inspired by this, we employ an HGJB to improve the operational stability of the micro-pump, conduct theoretical modeling and analysis to explore its dynamic and static characteristics, and verify its effect through experiments.

In this work, we developed a herringbone grooved structure on a journal bearing applied in a micro-pump. The comprehensive effect of herringbone grooves on water-lubricated journal bearings is studied numerically and experimentally. By CFD simulation, the pressure distribution and bearing capacity of the HGJB and PJB at different eccentricities are studied comparatively. Moreover, based on the perturbation method, the stiffness and damping coefficients are solved to clarify the rotor dynamic characteristics. Then, the critical mass is obtained by solving the rigid body motion equation, and the stability of the HGJB and PJB is evaluated. Finally, the veracity of the theoretical analysis is verified by experiments.

2 Operating principle of the hydraulic suspension micro-pump with the PJB and the HGJB

Figure 1 shows the structure of the hydraulic suspension micro-pump with the radial suspension bearing proposed in our previous work [18,19,37]. The journal bearing is composed of a rotor inside a sleeve, with a small clearance between them for fluid flow. Due to the eccentric placement of the journal, when the journal rotates, the thickness of the liquid film changes along the direction of rotation, forming a convergent region (part I in Figure 1) on the right side of line OO_1 and a diverging region (part II in Figure 1) on the left side. Due to the hydrodynamic effect, the liquid film of the convergent region generates high pressure, and the pressure of the diverging region decreases rapidly, thus constructing the pressure difference between the two regions and providing the radial suspension force.

The HGJB employed in this paper has a rectangular section, and the structure of the HGJB is shown in Figure 2. The main structural parameters are shown in Table 1, where the groove number n=12, helix angle β=45°, groove width l_g=0.6 mm and groove depth h_g=28.5 μm. It should be

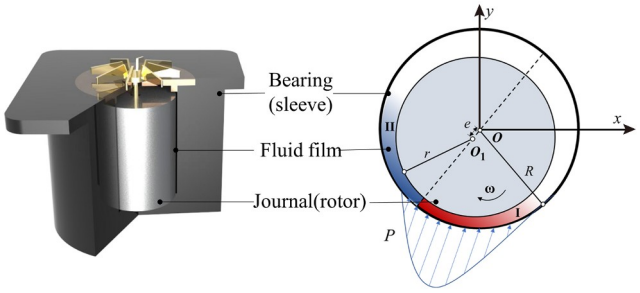

Figure 1 Schematic diagram of the journal bearing in the hydraulic suspension micro-pump.

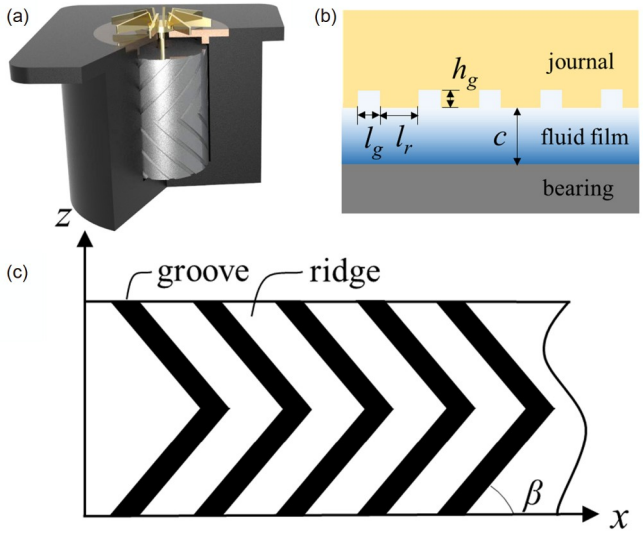

Figure 2 (a) 3D rendered graph of the HGJB in a micro-pump; (b) cross-sectional view of the HGJB; (c) radial expansion diagram of the herringbone grooved structure.

mentioned that the values of the groove number and helix angle are referred to Wang's work [38], and the depth and width of the groove are determined by the machining precision. Thus, we believe that the working performance of the HGJB may be better if the geometrical parameters are optimized further.

3 Methods

3.1 Experimental setup

Distinctly, the stability of journal bearings can be reflected by the journal's whirl tail. To observe it accurately, a test facility is constructed, and Figure 3(a) shows the overall schematic diagram of the test facility. To measure the real-time position of the journal, two laser displacement sensors (Keyence, LK-H020) with ±1 μm accuracy are installed on two micro-displacement stages (LD60-LM-2). The HGJB is assembled into a micro-pump with acrylic volute, whose transmissivity is high (more than 90%), allowing the laser to flash on the bearing. The inlet and outlet tubes of the micro-pump are connected to a water sink. To reduce the interference of external vibrations and ensure sufficient levelness, the working micro-pump is installed on a specific fixture, and the entire test facility is installed on a high-precision optical platform.

The test principle in this work is shown in Figure 3(b). Two laser displacement sensors are arranged vertically in the radial direction of the micro-pump. The laser flashes on the journal through the acrylic volute, and then the reflected light returns to the receiver. The data x_0 and y_0 are directly recorded by laser displacement sensors. The momentary po-

Table 1 Structure parameters of the PJB and HGJB

Type	Length l (mm)	Radius r (mm)	Clearance c (mm)	n	β (°)	l_g (mm)	h_g (μm)
PJB	17.2	6.33	0.07	–	–	–	–
HGJB	17.2	6.33	0.07	12	45	0.6	28.5

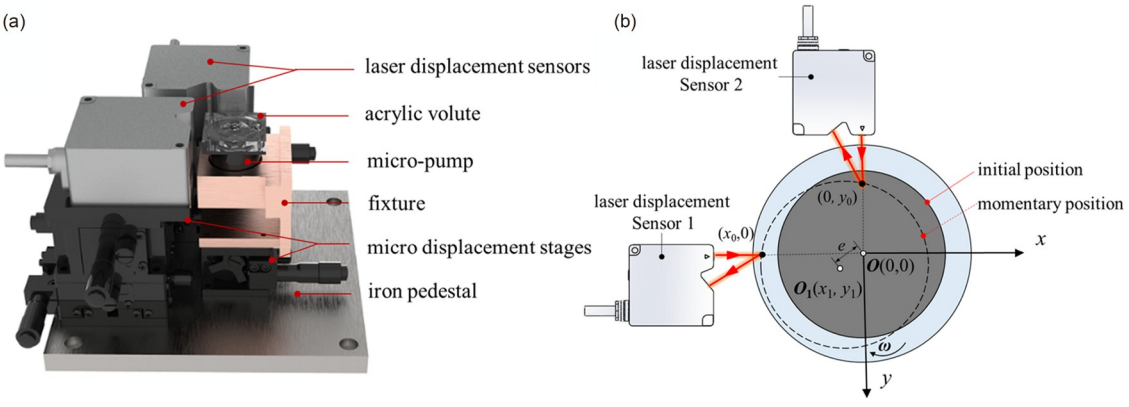

Figure 3 (a) Overall schematic diagram of the test facility; (b) schematic diagram of the experimental test principle.

sition (x_1, y_1) of the rotor can be calculated by combining eqs. (1) and (2), and the eccentricity e is denoted below.

$$(x_0 - x_1)^2 + (0 - y_1)^2 = r^2, \tag{1}$$

$$(0 - x_1)^2 + (y_0 - y_1)^2 = r^2, \tag{2}$$

$$e = \sqrt{x_1^2 + x_2^2}. \tag{3}$$

3.2 Numerical simulation

Numerical simulations are conducted to investigate the dynamic coefficients and pressure distributions of the HGJB and the PJB by COMSOL MULTIPHYSICS 5.6. Figure 4 shows the journal film domains of the PJB and the HGJB used in the simulation. Structured meshes are used for the PJB, and unstructured meshes are used for the HGJB. As shown in Figure 4, to capture the fluid flow process and pressure distribution details, grids are meshed finer in the herringbone groove zone. The pressure boundary condition of the inlet and outlet is set to zero pressure. The flow state of the liquid is judged by the critical Reynolds number formula of the concentric cylinder in eq. (4) [39]. The Reynolds numbers of the PJB and HGJB are calculated as follows:

$$Re_c = 41.1\sqrt{\frac{R}{C}}, \tag{4}$$

$$Re = \frac{\rho u d}{\mu}. \tag{5}$$

In this simulation, 20°C water is used as a lubricant, and the density and dynamic viscosity are set to 998.2 kg/m^3 and 1.006 mPa s, respectively. The grid independence tests are performed at a rotating speed of 15000 r/min and eccentricity of 0.1. The maximum pressures of the HGJB are calculated with grid numbers 41836, 132184, 443867, and 737229. The results are shown in Table 2. Similarly, the grid independence results of the PJB are shown in Table 2. Taking computation cost into consideration, the mesh scheme with a grid number of 443867 is used for the HGJB, while a grid number of 2400 is used for the PJB.

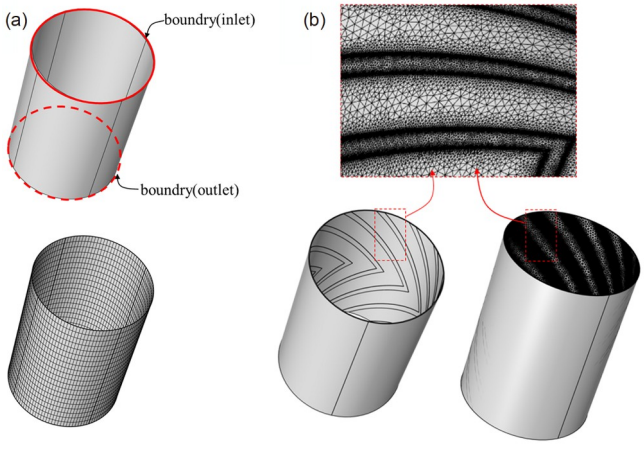

Figure 4 Simulation models of the PJB (a) and the HGJB (b).

3.3 Numerical method verification

Based on the numerical simulation method mentioned earlier, the performance of journal bearings is studied. To validate this method, six cases are studied, and the numerical results are compared with the experimental data of Gao and Yin's work [40].

Gao and Yin's experiment used 20°C water as a lubricant to test the eccentricity of bearings under six working conditions, as listed in Table 3, including different rotating speeds and loads. Figure 5 is a comparison of the numerical calculation results and Gao and Yin's experimental data

Table 2 Grid independence verification results of the HGJB and PJB

HGJB		PJB	
Grid number	Max pressure	Grid number	Max pressure
41836	6066.5	2400	3170.6
132184	6069.8	3200	3170.6
443867	6074.9	4800	3170.6
737229	6077.1	6400	3170.6

Table 3 Working conditions of Gao and Yin's experiment

Case	Rotating speed (r/min)	Load (N)
1	1500	2050
2	2000	2700
3	2500	3350
4	3000	3950
5	3500	4850
6	4000	5200

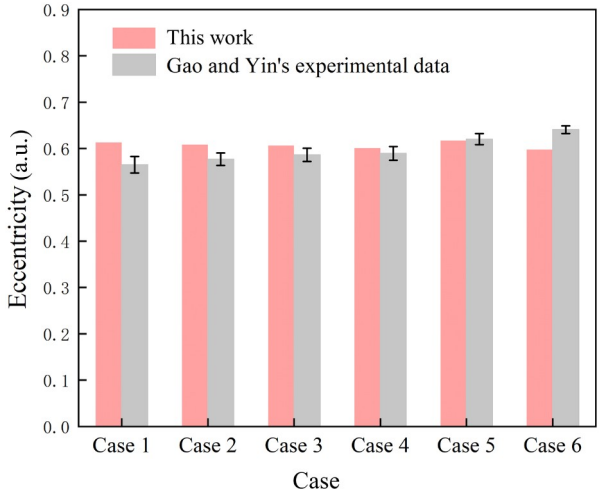

Figure 5 Comparison of numerical results with experimental data.

under six working conditions. The results show that the numerical calculation results match well with the experimental data, and the maximum error is less than 8.45%.

3.4 Rotor dynamic calculation

From the viewpoint of rotor dynamics, the liquid film usually acts as a nonlinear spring and damper, which has a great influence on the dynamic characteristics of the whole system. In the study of journal bearings, because most of them involve only small or infinitesimal amplitudes, the stiffness coefficient and damping characteristics of the liquid film are considered to be linear.

Assuming that the journal is in static equilibrium, a Taylor expansion is carried out for the bearing capacity in the x and y directions. After ignoring higher-order terms, the bearing capacity is given as follows:

$$F_x = F_{x0} + \left(\frac{\partial F_x}{\partial x}\right)_0 \Delta x + \left(\frac{\partial F_x}{x\partial y}\right)_0 x\Delta y + \left(\frac{\partial F_x}{\partial x'}\right)_0 x' + \left(\frac{\partial F_x}{x\partial y'}\right)_0 xy',$$
$$F_y = F_{y0} + \left(\frac{\partial F_y}{\partial x}\right)_0 \Delta x + \left(\frac{\partial F_y}{x\partial y}\right)_0 x\Delta y + \left(\frac{\partial F_y}{\partial x'}\right)_0 x' + \left(\frac{\partial F_y}{x\partial y'}\right)_0 xy'. \tag{6}$$

It can be seen that the coefficient of the original term in eq. (6) has a stiffness dimension, and the coefficient of the first-order term has a damping dimension. After simplification, it can be expressed by eq. (7):

$$\begin{pmatrix}\Delta F_x\\ \Delta F_y\end{pmatrix} = \begin{pmatrix}K_{xx} & K_{xy}\\ K_{yx} & K_{yy}\end{pmatrix}\begin{pmatrix}\Delta x\\ \Delta y\end{pmatrix} + \begin{pmatrix}C_{xx} & C_{xy}\\ C_{yx} & C_{yy}\end{pmatrix}\begin{pmatrix}x'\\ y'\end{pmatrix}, \tag{7}$$

where K_{xx} and K_{yy} are direct stiffness coefficients, K_{xy} and K_{yx} are cross stiffness coefficients, C_{xx} and C_{yy} are direct damping coefficients, C_{xy} and C_{yx} are cross damping coefficients, Δx and Δy are displacements, and x' and y' are the velocities. The dynamic characteristics of the HGJB and the PJB are calculated by the pressure perturbation method [41]. The calculation method is denoted as follows:

$$K_{xx} = \frac{\Delta F_{sxx}}{\Delta x}, K_{xy} = \frac{\Delta F_{sxy}}{\Delta y},$$
$$K_{yx} = \frac{\Delta F_{syx}}{\Delta x}, K_{yy} = \frac{\Delta F_{syy}}{\Delta y}, \tag{8}$$

$$C_{xx} = \frac{\Delta F_{vxx}}{x'}, C_{xy} = \frac{\Delta F_{vxy}}{y'},$$
$$C_{yx} = \frac{\Delta F_{vyx}}{x'}, C_{yy} = \frac{\Delta F_{vyy}}{y'}. \tag{9}$$

In eq. (8), ΔF_{sij} is the variation in fluid film capacity caused by displacement perturbation, $\Delta F_{sij}=F_{sij}-F'_{sij}$, where F_{sij} is the liquid film capacity in the equilibrium state, and F'_{sij} is the liquid film capacity after the displacement perturbation is applied. In eq. (9), ΔF_{vij} is the variation in the fluid film capacity caused by the velocity perturbation. $\Delta F_{vij}=F_{vij}-F'_{vij}$, where F_{vij} is the liquid film capacity in the equilibrium state, and F'_{vij} is the liquid film capacity after the velocity perturbation is applied.

The dynamic characteristic parameters of liquid films are very important for studying the stability of journal bearings. Generally, the larger the stiffness of the liquid film is, the stronger the bearing capacity, and the larger the damping is, the better the stability. Furthermore, the influence of stiffness and damping need to be considered simultaneously when studying the stability of a journal bearing, and the optimization approach must be based on the coupling effect between them to achieve the best stability. The system stability is characterized by the critical journal mass, which is determined by the stiffness coefficient, damping coefficient, and journal mass. By substituting eq. (6) into instantaneous dynamic eq. (10):

$$mx'' + \Delta F_x = 0,$$
$$my'' + \Delta F_y = 0. \tag{10}$$

The dynamical equation of journal bearings can be expressed as eq. (11):

$$mx'' + K_{xx}\Delta x + K_{xy}\Delta y + C_{xx}x' + C_{xy}y' = 0,$$
$$my'' + K_{yx}\Delta x + K_{yy}\Delta y + C_{yx}x' + C_{yy}y' = 0. \tag{11}$$

Eq. (11) is a linear equation whose general solution is shown below, where v is the eigenvalue and is a complex number.

$$\Delta x = x_0 e^{vt},$$
$$\Delta y = y_0 e^{vt}. \tag{12}$$

By substituting eq. (12) into eq. (11), the characteristic equation is given as

$$(mv^2 + C_{xx}v + K_{xx})x_0 + (C_{xy}v + K_{xy})y_0 = 0,$$
$$(C_{yx}v + K_{yx})x_0 + (mv^2 + C_{yy}v + K_{yy})y_0 = 0. \tag{13}$$

In the critical state, there exists an eigenvalue v that is a pure imaginary number. Here, $v=i\omega_{st}$, and v is substituted into eq. (10); it can be expressed as

$$\Delta F_x = m\omega_{st}^2 x_0 e^{i\omega_{st}t} = m\omega_{st}^2 \Delta x,$$
$$\Delta F_y = m\omega_{st}^2 y_0 e^{i\omega_{st}t} = m\omega_{st}^2 \Delta y, \tag{14}$$

where ω_{st} is the critical whirl frequency. In the critical state, the proportional coefficient between ΔF_x and Δx, ΔF_y and Δy is $m\omega_{st}^2$. This indicates that the liquid film at this time is equivalent to an isotropic spring with similar dynamic characteristics, and its stiffness is called the equivalent stiffness, which is expressed by K_{eq} as follows:

$$K_{eq} = m\omega_{st}^2. \tag{15}$$

By substituting eq. (15) and $v=i\omega_{st}$ into eq. (13), we obtain

$$(i\omega_{st}C_{xx} + K_{xx} - K_{eq})x_0 + (i\omega_{st}C_{xy} + K_{xy})y_0 = 0,$$
$$(i\omega_{st}C_{yy} + K_{yy})x_0 + (i\omega_{st}C_{yx} + K_{yx} - K_{eq})y_0 = 0. \tag{16}$$

For eq. (16), only when a nontrivial solution exists will the determinant of the coefficients equal 0. Then, the motion of the rotor converges. The convergence criterion of the rotor can be expressed as follows:

$$\begin{vmatrix} \mathrm{i}\omega_{st}C_{xx}+K_{xx}-K_{eq} & \mathrm{i}\omega_{st}C_{xy}+K_{xy} \\ \mathrm{i}\omega_{st}C_{yx}+K_{yx} & \mathrm{i}\omega_{st}C_{yy}+K_{yy}-K_{eq} \end{vmatrix} = 0, \tag{17}$$

where the equivalent stiffness K_{eq} and the critical whirl frequency ω_{st} can be obtained by expanding the determinant:

$$\begin{aligned} K_{eq} &= \frac{K_{xx}C_{yy}+K_{yy}C_{xx}-K_{xy}C_{yx}K_{yx}C_{xy}}{C_{xx}+C_{yy}}, \\ \omega_{st}^2 &= \frac{(K_{eq}-K_{xx})(K_{eq}-K_{yy})-K_{xy}K_{yx}}{C_{xx}C_{yy}-C_{xy}C_{yx}}, \end{aligned} \tag{18}$$

where K_{eq} reflects the comprehensive stiffness of the liquid film and ω_{st} reflects the development degree of whirl in the liquid film. When the other conditions are consistent, if K_{eq} is larger and ω_{st} is smaller, the stability of the rotor-bearing system is better. Obviously, the equivalent stiffness coefficient of the liquid film should always be greater than zero, and $K_{eq} > 0$ is a necessary condition for system stability. When $\omega_{st} < 0$, even if a perturbation is applied, the whirl will decay quickly; hence, $\omega_{st} < 0$ is a sufficient condition for system stability. Only when $K_{eq} > 0$ and $\omega_{st} > 0$ does the system seem to be unstable. As follows, the ratio of K_{eq} to ω_{st}^2 is the critical journal mass, which is the key indicator for system stability.

$$m_c = \frac{K_{eq}}{\omega_{st}^2}. \tag{19}$$

If the actual mass of the rotor is greater than m_c, the rotor motion is divergent, and the system is unstable. In contrast, the rotor motion is convergent, and the system is stable. Furthermore, the larger m_c is, the higher the stability margin of the system is.

4 Results and discussion

Simulations are carried out at 15000 r/min, which is the typical working speed of this micro-pump. The pressure distribution, bearing capacity, and dynamic coefficients of the HGJB and PJB when the eccentricity is 0.1–0.9 are investigated by numerical simulations. Taking the eccentricity of 0.1 as an example, the pressure distribution of the HGJB and PJB are shown in Figure 6(a). It can be observed that the hydrodynamic effect of fluid causes a positive-pressure region and a negative-pressure region on the journal surface. It is evident that HGJB produces a higher pressure at the cusp of the herringbone groove than at the same position of the PJB. Figure 6(b) shows the pressure distribution of the intermediate plane on the HGJB and PJB. The maximum and minimum pressures of the PJB are 3170.7 and −3170.7 Pa, which are symmetrically distributed in the convergent region and diverging region, respectively. The maximum pressure of the HGJB is 8096 Pa, and the minimum pressure is −1784 Pa. There are twelve pressure peaks on the HGJB, which correspond to twelve herringbone grooves on the journal surface. The reason for this phenomenon is that the herringbone grooves restrict the fluid flow in the bearing clearance, and the fluid converges at the cusps, making the local pressure higher than around.

As shown in Figure 7, with increasing eccentricity, the bearing capacity and maximum pressure of the HGJB and PJB increase sharply, while the minimum pressure decreases sharply. When the eccentricity increases, the minimum thickness of the liquid film decreases, and the gradient of the liquid film thickness in the bearing clearance increases, which enhances the hydrodynamic effect of the fluid. As a result, the pressure in the convergent region is higher, the pressure in the diverging region is lower, and the loading capacity is larger. The results show that when the eccentricity is less than 0.55, the minimum pressure of the HGJB is

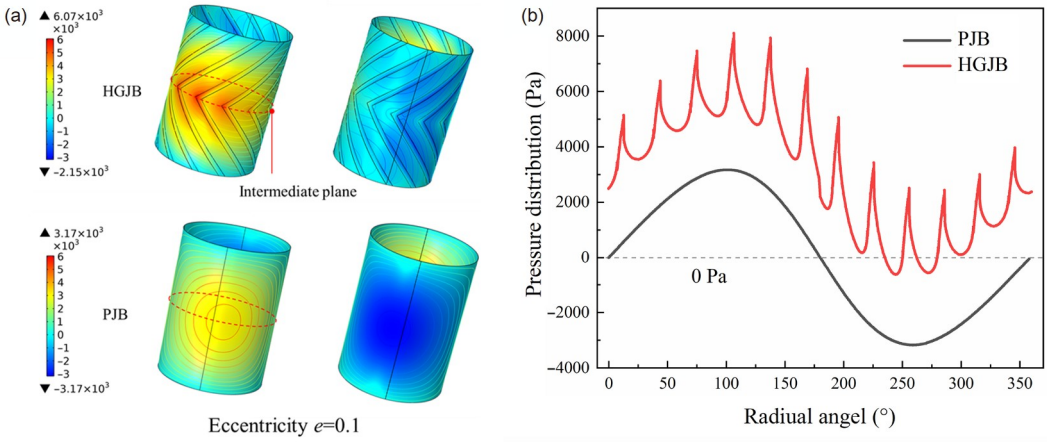

Figure 6 (a) Pressure distribution contours of the HGJB and PJB; (b) pressure distribution on the intermediate circle of the HGJB and PJB varies with the radial angle.

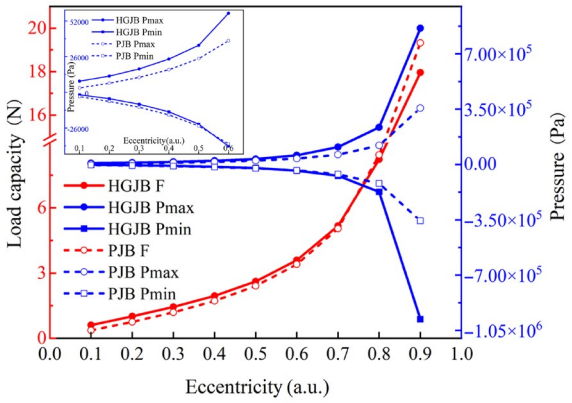

Figure 7 Journal bearing capacity and the maximum/minimum pressure of the HGJB and PJB vary with the eccentricity.

greater than that of the PJB, and the maximum pressure of the HGJB is always greater than that of the PJB. This indicates that the fluid pumping effect brought by the herringbone grooves enhances the positive pressure. Moreover, the force of the convergent region is enhanced while that of the diverging region is weakened. When the eccentricity is less than 0.74, the load capacity of the HGJB is greater than that of the PJB, and it is smaller than that of the PJB when the eccentricity is larger than 0.74. The reason for this phenomenon is that when the eccentricity is at the critical value of 0.74, the strengthening of the force in the convergent region will offset the weakening of the force in the diverging region, making the bearing capacity of the HGJB equal to PJB.

Figure 8 shows the variation in the stiffness coefficients and damping coefficients as the eccentricity varies. The results show that the absolute value of all stiffness coefficients, damping coefficients, and their growth rates increase with increasing eccentricity. The greater the eccentricity is, the stronger the hydrodynamic effect. Note that the larger the direct damping coefficients C_{xx} and C_{yy} are, the better the stability of the journal bearing in response to external disturbances. When the eccentricity is less than 0.5, the direct stiffness coefficients K_{xx} of the HGJB and PJB are approximately the same. Additionally, when the eccentricity is between 0.5–0.8, the direct stiffness coefficient K_{xx} of the HGJB is larger, while that of the PJB is larger when the eccentricity is larger than 0.8. The K_{yy} of the HGJB is greater than that of the PJB at all eccentricities. When the eccentricity is larger than 0.5, the K_{xy} of the PJB is much greater than that of the HGJB. When the eccentricity is less than 0.5, it is approximately the same as that of the HGJB. When the eccentricity is less than 0.28, the C_{xx} of the HGJB is greater than that of the PJB. When the eccentricity is less than 0.58, the C_{yy} of the HGJB is greater than that of the PJB.

Figure 9(a) shows the variation in the equivalent stiffness coefficients and critical whirl frequency as the eccentricity varies. The results show that with increasing eccentricity, the K_{eq} of the HGJB and PJB increases, and ω_{st} decreases. Consequently, it can be concluded that with increasing eccentricity, the stability of the rotor-bearing system increases. More specifically, when the eccentricity is greater than 0.8, the K_{eq} of the HGJB is greater than that of the PJB. When the

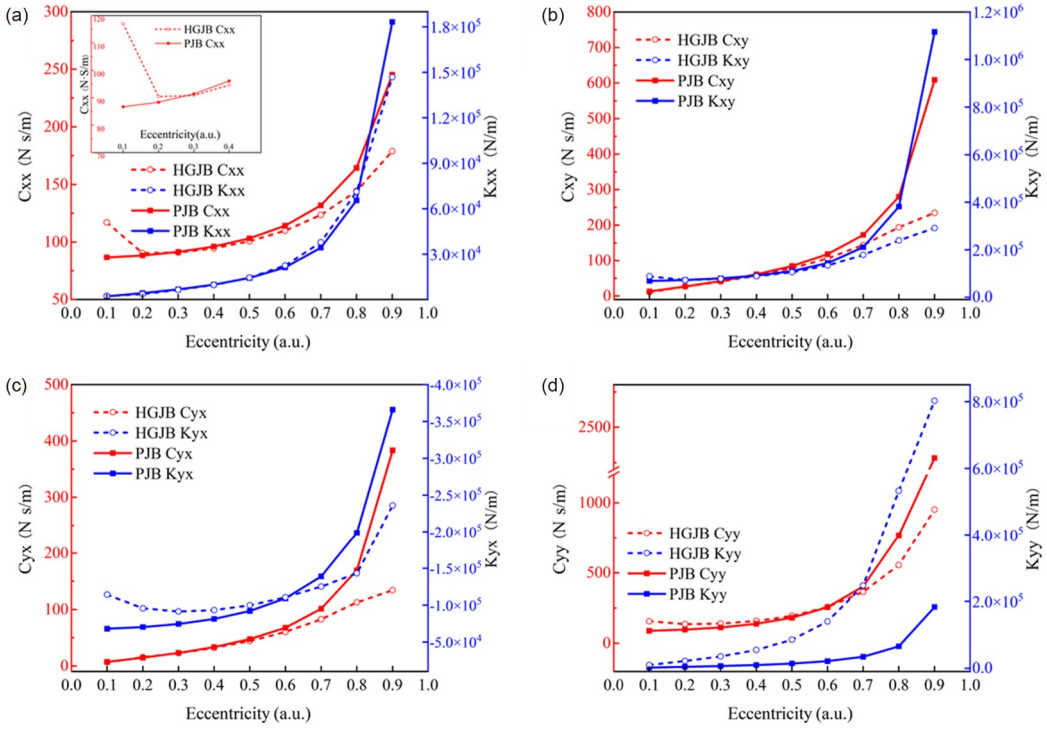

Figure 8 Dynamic stiffness coefficients K_{ij} and damping coefficients C_{ij} of the HGJB and PJB varying with the eccentricity.

eccentricity is greater than 0.8, the ω_{st} of the HGJB becomes imaginary, which means that it reaches an absolutely stable state. The same is true for the PJB when the eccentricity is greater than 0.84. The ω_{st} of the HGJB is smaller than that of the PJB at all eccentricities. The abovementioned results show that the HGJB is more stable than the PJB in a certain range of eccentricity. To find this range precisely, the stabilities of both can be characterized by the critical journal mass m_c. As shown in Figure 9(b), when the eccentricity is less than 0.7, the m_c of the HGJB is larger than that of the PJB. This means that the HGJB is more stable than the PJB when the rotor mass is the same. When the eccentricity exceeds 0.84, the m_c of both become negative, and the systems reach stable states.

Figure 10 shows the details of the HGJB used in the experiment. As shown in Figure 10, the HGJB was successfully fabricated by applying chemical etching technology. Figure 10(a) and (b) show the top view of the HGJB. The average width of the groove is 612.25 μm, which is slightly greater than the designed value of 600 μm, and the helix angle is 45°. To characterize the effective depth of the groove, an ultra-depth three-dimensional micro-scope (Keyence, VHX-7000) was employed. The red line in Figure 10(a) represents the location of the longitudinal section, which spans the groove and the ridge. Figure 10(c) shows the absolute height distribution of the journal surface on the longitudinal section along the red line. The groove is approximately horizontal, and there is an obvious height difference between the groove and the ridge. By calculating the average height difference between the groove and the ridge, the depth of the groove is 28.54 μm.

To verify the conclusion of the numerical simulation, a laser displacement experiment is carried out. The journal radius used in the experiment is 6.33 mm, and the sleeve radius is 6.4 mm. The liquid lubricant is distilled water at 20°C, and the journal rotating speed is set to 15000 r/min. The sampling frequency of the laser displacement sensor is 20 kHz, and the time interval between adjacent sampling points is 50 μs. We measure the displacement of the journals in the x and y directions, and 10000 data points are collected in each group.

Typically, as shown in Figure 11, displacement-time responses within ten periods are selected for discussion. The amplitude and period of whirls of the HGJB and PJB are

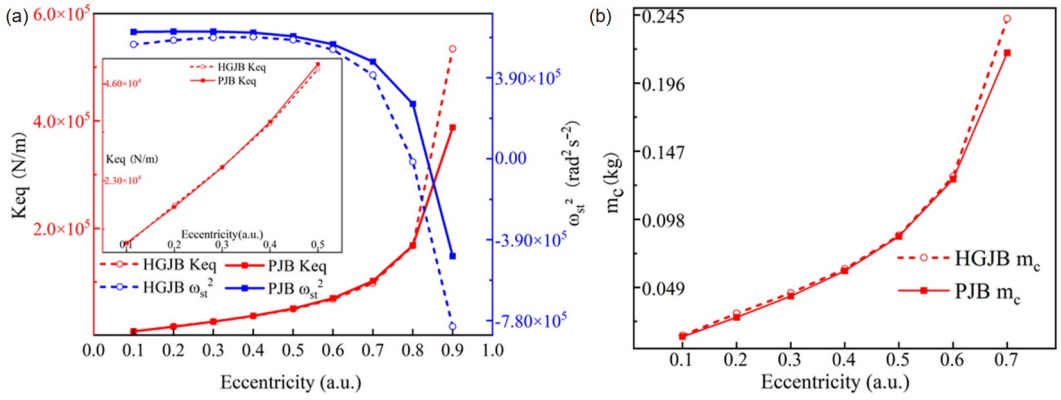

Figure 9 (a) Equivalent stiffness coefficient K_{eq} and critical whirl frequency ω_{st} of the HGJB and PJB vary with eccentricity; (b) critical journal masses (m_c) of the HGJB and PJB vary with eccentricity.

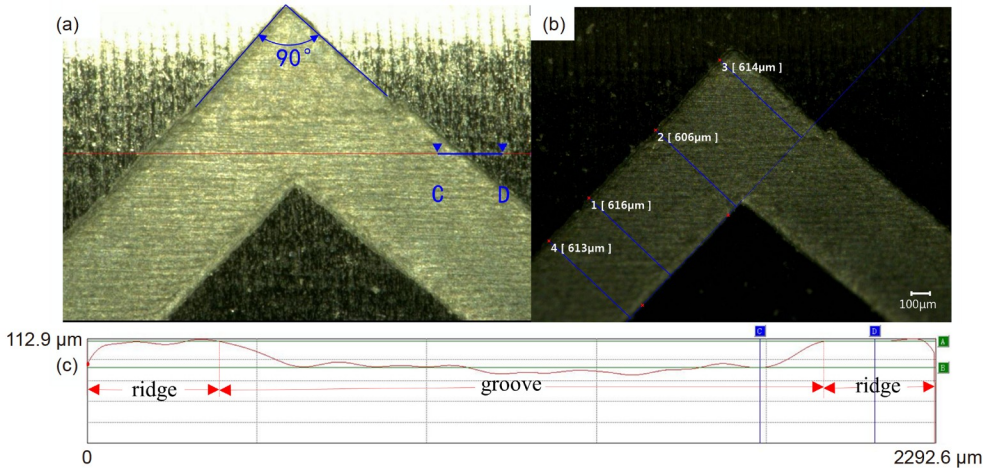

Figure 10 (a), (b) Top views of the fabricated HGJB prototype; (c) absolute height distribution of the longitudinal section.

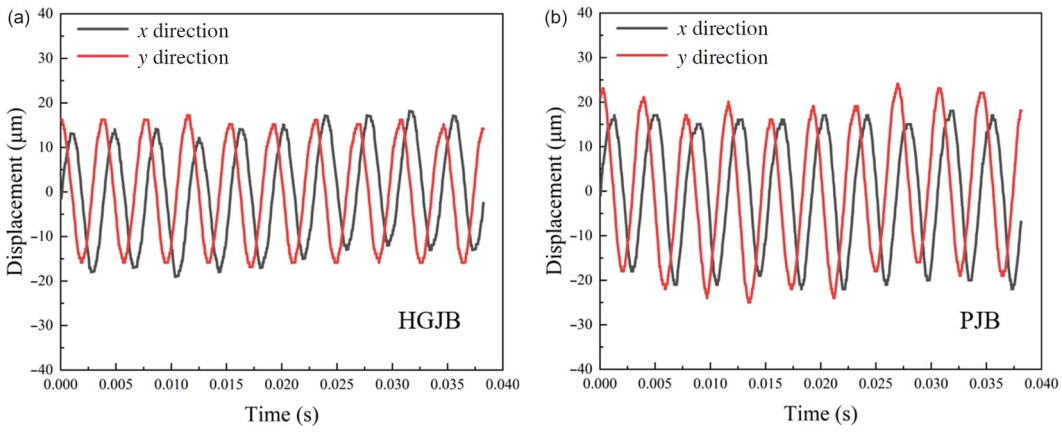

Figure 11 Displacement in the x direction and y direction of the HGJB and PJB.

relatively fixed, but the absolute values of the peaks and valleys of each cycle are constantly changing, which indicates that the whirl center is constantly changing. Moreover, the whirl amplitude of the journal of the PJB is larger than that of the HGJB, which indicates that the herringbone groove inhibits the whirl range of the rotor. The eccentricity variations in the journals in the above period are schematically shown in Figure 11. The eccentricity is calculated as $e=r/c$. The calculation method of whirl radius r is as follows. It can be seen from Figure 11 that both journals are moving elliptically around the origin of the sleeve. The HGJB has a smaller eccentricity, which is on average 16.87% less than that of the PJB.

$$r = \frac{1}{n}\sum_{1}^{n}\sqrt{\left(x_i - \frac{1}{n}\sum_{1}^{n}x_i\right)^2 + \left(y_i - \frac{1}{n}\sum_{1}^{n}y_i\right)^2}. \quad (20)$$

From the initial analysis of Figure 11, it can be inferred that the journal's whirl center is changing periodically. To investigate the regularity of the rotor's trajectory over a long period, the trajectory figure is drawn with a time interval of 0.5 s, as shown in Figures 12 and 13. The whirl centers of the HGJB and PJB are constantly changing, but both are limited within a certain range. Moreover, the HGJB is more stable with its smaller whirl range. The long-term whirl amplitude of the HGJB in the x direction is 40.13 μm, which is much lower than that of the PJB, which is 57.01 μm. In the y direction, the whirl amplitude of the HGJB is 37.98 μm, which is much lower than that of the PJB, which is 50.03 μm. The eccentricities of the HGJB and PJB within 0.5 s were calculated to be 0.222 and 0.276, respectively. From the above experimental test results, it can be observed that under the test conditions, the stability of the HGJB is better than that of the PJB, which is consistent with the results of the theoretical calculation.

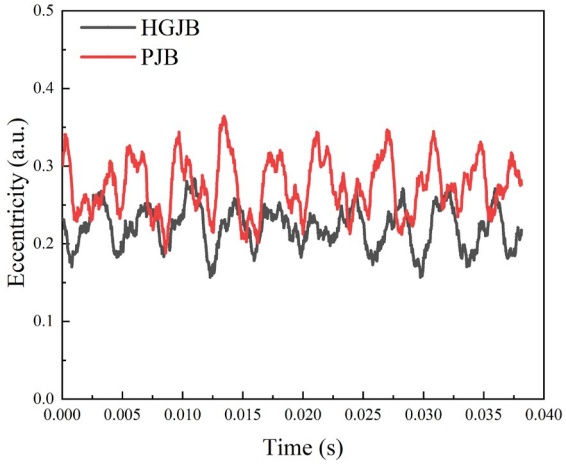

Figure 12 Eccentricities of the HGJB and PJB vary with time.

5 Conclusion

In this work, we developed a HGJB for the hydraulic suspension micro-pump. The CFD simulation and rotor dynamics calculation were combined to compare the dynamic and static characteristics of the HGJB and PJB. The results show that the HGJB has better working performance in a specific range of eccentricities, which can be explained by the pumping effect caused by the herringbone groove. Furthermore, the rotor dynamics calculation shows that the HGJB has better operational stability than the PJB when the eccentricity is less than 0.4 and greater than 0.62. We fab-

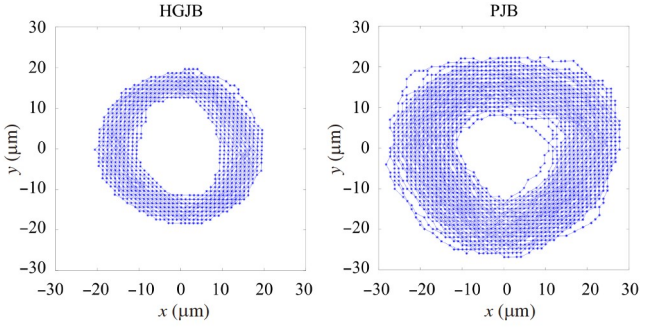

Figure 13 Whirl trajectories of the HGJB and PJB within 0.5 s.

ricated a prototype of the HGJB and established a set of laser displacement testing facilities to observe the trajectory of the journal in the HGJB and PJB. According to the experimental results, the operational stability of the HGJB is stronger than that of the PJB at the typical working speed of the micro-pump. The whirl range of the journal decreases by 29.61% in the x direction and by 24.09% in the y direction. Therefore, it can be concluded that the herringbone grooved structure can significantly suppress the whirl of the journal, reducing the risk of contact wear. HGJBs have a positive effect on improving the operational stability of hydraulic suspension micro-pump.

This work was supported by the Open Fund of Science and Technology on Thermal Energy and Power Laboratory (Grant No. TPL 2019B03).

1 Nisar A, Afzulpurkar N, Mahaisavariya B, et al. MEMS-based micropumps in drug delivery and biomedical applications. Sens Actuat B-Chem, 2008, 130: 917–942
2 Tsai N C, Sue C Y. Review of MEMS-based drug delivery and dosing systems. Sens Actuat A-Phys, 2007, 134: 555–564
3 Morshuis M, El-Banayosy A, Arusoglu L, et al. European experience of DuraHeart™ magnetically levitated centrifugal left ventricular assist system. Eur J Cardio-Thoracic Surg, 2009, 35: 1020–1028
4 Morshuis M, Schoenbrodt M, Nojiri C, et al. DuraHeart™ magnetically levitated centrifugal left ventricular assist system for advanced heart failure patients. Expert Rev Med Devices, 2010, 7: 173–183
5 Luo X B, Hu R, Liu S, et al. Heat and fluid flow in high-power LED packaging and applications. Prog Energy Combust Sci, 2016, 56: 1–32
6 Wu R K, Fan Y W, Hong T, et al. An immersed jet array impingement cooling device with distributed returns for direct body liquid cooling of high power electronics. Appl Thermal Eng, 2019, 162: 114259
7 Liu P, Ren T T, Ge Y L, et al. Performance analyses of a novel finned parabolic trough receiver with inner tube for solar cascade heat collection. Sci China Tech Sci, 2023, 66: 1417–1434
8 Zhang J J, Chen Y W, Liu Y, et al. Experimental investigation on heat transfer characteristics of microcapsule phase change material suspension in array jet impingement. Sci China Tech Sci, 2022, 65: 1634–1645
9 Mohith S, Karanth P N, Kulkarni S M. Recent trends in mechanical micropumps and their applications: A review. Mechatronics, 2019, 60: 34–55
10 Li H Y, Liu J K, Li K, et al. A review of recent studies on piezoelectric pumps and their applications. Mech Syst Signal Process, 2021, 151: 107393
11 Wang X Y, Cheng C, Wang S L, et al. Electroosmotic pumps and their applications in microfluidic systems. Microfluid Nanofluid, 2009, 6: 145–162
12 Johnson M J, Go D B. Recent advances in electrohydrodynamic pumps operated by ionic winds: A review. Plasma Sources Sci Technol, 2017, 26: 103002
13 Yang H, Jia H, Zhu C H, et al. Review of the hydraulic and structural design of high-speed centrifugal pumps. Front Energy Res, 2022, 10: 899093
14 Wang C Y, Wang F J, An D S, et al. A general alternate loading technique and its applications in the inverse designs of centrifugal and mixed-flow pump impellers. Sci China Tech Sci, 2021, 64: 898–918
15 Yamane T. The present and future state of nonpulsatile artificial heart technology. J Artif Organs, 2002, 5: 149–155
16 Pagani F D. Continuous-flow rotary left ventricular assist devices with "3rd generation" design. Semin Thorac Cardiovasc Surg, 2008, 20: 255–263
17 Kink T, Reul H. Concept for a new hydrodynamic blood bearing for miniature blood pumps. Artif Organs, 2004, 28: 916–920
18 Wu R K, Duan B, Liu F L, et al. Design of a hydro-dynamically levitated centrifugal micro-pump to the active liquid cooling system. In: Proceedings of the 18th International Conference on Electronic Packaging Technology (ICEPT). Harbin, 2017. 402–406
19 Luo X B, Liu F L, Duan B, et al. Micro hydraulic suspension mechanical pump. US Patent. 10495093B2, 2017-01-19
20 Kumar S, Kumar V, Singh A K. Influence of lubricants on the performance of journal bearings—A review. Tribol-Mater Surfs Interfaces, 2020, 14: 67–78
21 Garg H C, Sharda H B, Kumar V. On the design and development of hybrid journal bearings: A review. Tribotest, 2006, 12: 1–19
22 Tian L, Wang W J, Peng Z J. Nonlinear effects of unbalance in the rotor-floating ring bearing system of turbochargers. Mech Syst Signal Processing, 2013, 34: 298–320
23 Chen S K, Chou H C, Kang Y. Stability analysis of hydrodynamic bearing with herringbone grooved sleeve. Tribol Int, 2012, 55: 15–28
24 Gad A M, Nemat-Alla M M, Khalil A A, et al. On the optimum groove geometry for herringbone grooved journal bearings. J Tribol, 2006, 128: 585–593
25 Ku C P R. Dynamic characteristics of hard disk drive spindle motors-comparison between ball bearings and hydrodynamic bearings. J Tribol, 1996, 118: 402–406
26 Zhu J, Ono K. A comparison study on the performance of four types of oil lubricated hydrodynamic thrust bearings for hard disk spindles. J Tribol, 1999, 121: 114–120
27 Xu J H, Jiao C X, Zou D L, et al. Study on the dynamic behavior of herringbone gear structure of marine propulsion system powered by double-cylinder turbines. Sci China Tech Sci, 2022, 65: 611–630
28 Hirayama T, Yamaguchi N, Sakai S, et al. Optimization of groove dimensions in herringbone-grooved journal bearings for improved repeatable run-out characteristics. Tribol Int, 2009, 42: 675–681
29 Muijderman E A. Spiral groove bearings. Ind Lubr Tribol, 1965, 17: 12–17
30 Sahu M, Sarangi M, Majumdar B C. Thermo-hydrodynamic analysis of herringbone grooved journal bearings. Tribol Int, 2006, 39: 1395–1404
31 Han Y, Xiong S, Wang J, et al. A new singularity treatment approach for journal-bearing mixed lubrication modeled by the finite difference method with a herringbone mesh. J Tribol, 2016, 138: 011704
32 Zirkelback N, San Andres L. Finite element analysis of herringbone groove journal bearings: A parametric study. J Tribol, 1998, 120: 234–240
33 Jang G H, Yoon J W. Nonlinear dynamic analysis of a hydrodynamic journal bearing considering the effect of a rotating or stationary herringbone groove. J Tribol, 2002, 124: 297–304
34 Hirs G G. The load capacity and stability characteristics of hydrodynamic grooved journal bearings. A S L E Trans, 1965, 8: 296–305
35 Gao S Y, Shi Y G, Xu L S, et al. Investigation on influences of herringbone grooves for the aerostatic journal bearings applied to ultra-high-speed spindles. Proc Inst Mech Eng C-J Mech Eng Sci, 2019, 233: 5795–5812
36 Ikeda S, Arakawa Y, Hishida N, et al. Herringbone-grooved bearing with non-uniform grooves for high-speed spindle. Lubrication Sci, 2010, 22: 377–392
37 Xing G Y, Xue S, Hong T, et al. A novel hydrodynamic suspension micropump using centrifugal pressurization and the wedge effect. Sci China Tech Sci, 2023, 66: 2047–2058
38 Wang B, Sun Y T, Ding Q. Dynamic characteristics of the herringbone groove gas journal bearings: Numerical simulations. Shock Vib, 2016, 2016: 1–13
39 Taylor G I. VIII. Stability of a viscous liquid contained between two rotating cylinders. Phil Trans R Soc Lond A, 1923, 223: 289–343
40 Gao G, Yin Z, Jiang D, et al. Numerical analysis of plain journal bearing under hydrodynamic lubrication by water. Tribol Int, 2014, 75: 31–38
41 Rowe W B, Chong F S. Computation of dynamic force coefficients for hybrid (hydrostatic/hydrodynamic) journal bearings by the finite disturbance and perturbation techniques. Tribol Int, 1986, 19: 260–271